Theoretical Ecology (2018) 11:333–350
https://doi.org/10.1007/s12080-018-0370-7

ORIGINAL PAPER

Production of nitrate spikes in a model of ammonium biodegradation

I. R. Moyles[1] · A. C. Fowler[1,2]

Received: 27 September 2017 / Accepted: 4 February 2018 / Published online: 17 February 2018

Abstract
Nitrification at the site of a contaminant ammonium plume from a former coal carbonisation plant can be modelled with three competing bacterial populations of *Nitrosomonas*, *Nitrobacter*, and *Brocadia anammoxidans*. Oscillations of chemical species at the site can be explained by a reduced model of ammonium competition between *Nitrosomonas* and *B. anammoxidans* which effectively acts as an activator-inhibitor system. Stable oscillations occur in conditions of low nutrient (ammonium) supply and this causes a spatial travelling wave in a borehole profile when diffusion is introduced.

Keywords Ammonium plume · Nitrification · Spatial oscillations · Bacterial competition

Introduction

The remediation of contaminated groundwater by bacterial reaction, termed bioremediation, is a process of significant and enduring interest in industrial and agricultural settings. There is currently much interest in the quality of groundwater, much of it driven by legislation directives, and a recent study by Gleeson et al. (2015) has concluded that only approximately 6% of groundwater is renewable, which emphasises the importance of maintaining the resource. The problem of groundwater quality is an endemic one, since every industrialised country is littered with countless spills and leaks of various contaminants. Typically, the contaminated groundwater forms a plume, which then migrates slowly under the influence of the regional groundwater flow, and this causes water quality problems if the plume reaches streams or wells as it migrates.

However, almost any contaminant is subject to consumption and removal by bacterial colonies within the soil, and thus, bioremediation can affect clean-up of the pollutant. It is important to be able to predict whether such bioremediation will be effective, but it is clearly impractical to monitor the spread of the plume in a comprehensive manner. Borehole data is useful but expensive, and thus, numerical modelling can provide a cheap but effective means of predicting the spread of pollutants in the ground.

While this is routinely done, an issue that then arises is in confronting the model calculations with borehole data. This is not as simple a task as it might seem because the chemical profiles in the boreholes can be quite complicated. While variance can be ascribed to noise in the data, it is also natural to associate consistent trends to deterministic processes, and the task we set ourselves in this paper is to consider the extent to which mathematical models of bacterial reaction and reactant dispersion within soil can predict some of the detail of measured borehole data. It is important to emphasise that the aims of the model approach are to reproduce qualitative structures in borehole data but not to completely replicate a particular data set.

The Rexco site

The Rexco site near Mansfield in the UK is the site of a former coal carbonisation plant which was in operation between 1930 and 1970. Leakage from the plant caused a plume of phenols and ammonium to spread, but by the 1990s, the phenols had disappeared, leaving a plume of ammonium some 500 m long and 25 m deep, spreading at a rate of about 60 m year^{-1} in a north-easterly direction. Two boreholes were dug, at distances from the source of 65 m (bh 102) and 130 m (bh 101), and data of the chemical profiles has been reported by Smits et al. (2009), for example, with the site geochemistry described in Davison (1998). Figure 1

✉ I. R. Moyles
iain.moyles@ul.ie

A. C. Fowler
andrew.fowler@ul.ie

[1] MACSI, University of Limerick, Limerick, Ireland

[2] OCIAM, University of Oxford, Oxford, UK

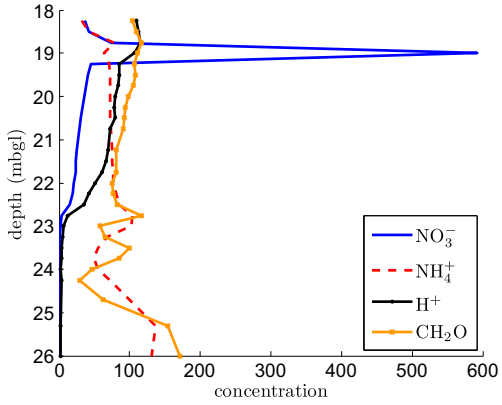

Fig. 1 Concentrations of NH_4^+ (ammonium), NO_3^- (nitrate), H^+ (acid), and CH_2O (organic carbon) as functions of depth below ground surface, measured in metres below ground level (mbgl) at borehole 102 on the Rexco site in Mansfield. Ammonium and nitrate concentrations are measured in mg L^{-1}, acid is measured in nmol L^{-1}, and organic carbon is measured in 1×10^{-5} mol L^{-1}. Data provided courtesy of Arne Hüttmann, GPRG, University of Sheffield

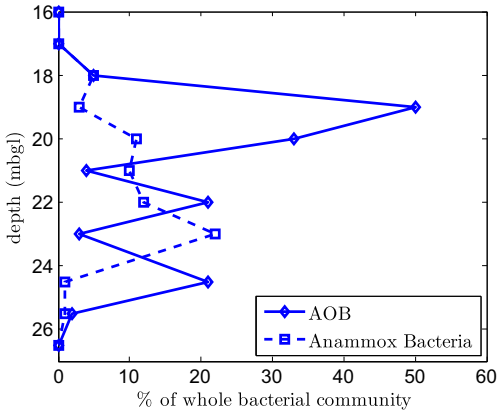

Fig. 3 Bacterial colony populations measured as a percentage of the total bacterial community as a function of depth below ground surface. AOB stands for ammonium-oxidising bacteria. This data is the bacterial companion to the chemistry data in Fig. 2 (redrawn from Smits et al. (2009))

shows data measured from bh 102 during the 1990s, while Fig. 2 shows data from the same borehole some ten years later. The horizontal axis represents depth in metres below ground level (the water table for both boreholes is at approximately 15 m below the surface). Figure 3 shows the bacterial colony data in the borehole corresponding to the chemistry in Fig. 2 and detailed in Smits et al. (2009).

In Fig. 1, a sharp nitrate front appears at a depth of 19 m and then a non-zero concentration persists until around 23 m where nitrate is removed entirely. Throughout this distance, there is a concurrent depletion of hydrogen ions as well; however, monitoring the acidity in the soil is beyond the scope of this paper and we make a remark about it in the conclusions. After the nitrate is depleted, ammonium and organic carbon CH_2O start to oscillate out of phase with each other. In earlier work by Fowler et al. (2014), Fowler (2014), and McGuinness et al. (2014), it was shown that bacterial populations competing for carbon resources can oscillate, thus providing a possible explanation for the oscillatory behaviour of the ammonium and carbon at the lower front. Figure 2, featuring the borehole data ten years later, also shows an early sharp nitrate spike. Since the second data set includes molecular oxygen content, we can see that this nitrate spike forms from the oxidation of ammonium by oxygenated groundwater. After this primary nitrate spike, the oxygen has been depleted, and secondary oscillations can be observed between nitrate and ammonium in the anaerobic regime. The absence of these apparent oscillations in Fig. 1 does not mean they were not occurring but perhaps the data resolution was not sufficient to detect them.

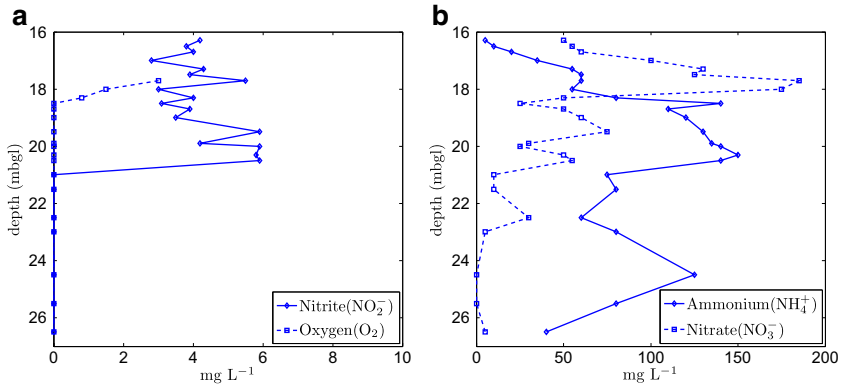

Fig. 2 **a** Concentrations of NO_2^- (nitrite) and O_2 (oxygen) and **b** Concentrations of NH_4^+, NO_3^-. Concentrations are functions of depth below ground surface measured in metres below ground level at borehole 102 on the Rexco site in Mansfield, ten years after the data in Fig. 1 (redrawn from (Smits et al. 2009)). Concentrations are measured in mg Lup-1

Modelling review and novelty

Mathematical nutrient modelling has a rich history of study and particular interest has been given to nitrogen as there are large health and environment impacts related to nitrogen gas emission and nitrate accumulation in groundwater. Much of the modelling effort has been given to large-scale, scenario-specific simulations with a focus on accurately capturing dynamics in bioreactors. For example, Capuno (2007) and Langergraber et al. (2009) consider a series of cascading chemical and biological reactions represented as ordinary differential equations with time-dependent concentrations. The work of Capuno (2007) was to analyse start-up reactors for nitrogen removal and simulations are made to provide insight into the underlying biological mechanisms. Langergraber et al. (2009) provides a 17-process model for the biokinetic processes in wetlands with the aims of being implemented as a surrogate for experimental insight. Other large-scale models such as Johnsson et al. (1987), Maggi et al. (2008), and Bailey et al. (2015) consider coupling reaction chemistry with advective-diffusive processes. The work of Maggi et al. (2008) for example solves nutrient concentration along with groundwater flow equations for water saturation while Johnsson et al. (1987) include a secondary model for soil temperature and flow as inputs to the nitrogen transformation equations. These models are calibrated with experimental data and simulations are computed followed by discussions of the dynamics. Abstract nutrient modelling has been carried out by Huisman and Weissing (1999) and conceptual numerical modelling carried out by Widdowson et al. (1988) and Kindred and Celia (1989). Huisman and Weissing (1999) present a set of k nutrients and j bacterial species. They show that the principle of competitive exclusion, where steady-state existence implies $k = j$, can be violated with nonlinear dynamics and oscillations in the population. The numerical simulations of Widdowson et al. (1988) and Kindred and Celia (1989) were designed to improve simulation techniques of nutrient transport and microbial activity.

The biggest strength of large-scale models is that they are designed to replicate experiments and can therefore produce simulations which accurately reflect collected data. However, a drawback of this approach is that the complexity limits clarity in exposing and understanding the dominant processes underlying the dynamics. Many qualitative structures such as oscillations are left unexplained or attributed to noise. Conversely, the abstract model of Huisman and Weissing (1999) provides an intimate connection between parameter values and the observed behaviour between competitive exclusion and oscillation but there is limited justification for parameter selection or understanding of the oscillatory mechanism. Furthermore, the generality of the model limits explicit dynamic transition conditions.

Our modelling approach follows a similar style to Fowler et al. (2014) which can be viewed as an intermediary between the general abstract modelling and large-scale complex modelling techniques. As in the latter models, we will posit equations based on specific nitrification biochemical reactions and analyse them through simulation. However, we will scale these models to produce non-dimensional numbers which will distinguish dominant and tertiary processes based on their size. We will use this technique to reduce the model to a simple set of equations amendable to analytic analysis in a similar manner to the abstract models.

The novelty of our modelling work is an accurate quantitative and predictive analysis of qualitative features observed in real borehole data. We explicitly show the dominant dynamics through a mathematical reduction of a larger-scale model which does not require any preconceived knowledge of the underlying processes, only relative values of key parameters. We explicitly determine the conditions under which competitive oscillations occur and precisely how they bifurcate from those of constant populations. We also identify the oscillatory mechanism by reducing a complex model to a classic differential equation of a harmonic oscillator, variants of which are well studied. Through the scaling and reduction method, our modelling approach and results can drastically reduce the complexity of large-scale systems, reducing computational costs while providing deeper insight into the problem.

Overall, in this paper, we seek to explain the form of the nitrate spike at the upper front, and its apparent evolution in Fig. 2 into a decaying oscillatory wave train. We propose that these oscillations are caused by the effect of the biochemical reactions on the interaction between the bacteria which are involved and in "Mathematical model", we postulate such a coupled model. We show a parameter regime in which the model can be reduced to a simple pair of oscillator equations. In "Temporal oscillations", we analyse a certain limit of the mathematical model to temporal oscillations, that is, we consider the nutrient and bacterial concentrations without any dispersive mechanism. To introduce the spatially oscillating wave train, we introduce nutrient diffusion in "Spatial oscillations". Implications of the model are discussed in "Discussion and conclusion".

Mathematical model

The oxidation of ammonium to nitrate is a process termed nitrification for which there are two main steps. Firstly, in a process termed nitritation, ammonium is converted to nitrite through a class of bacteria known as ammonium-oxidising

bacteria (AOB). Secondly, in nitratation, nitrite-oxidising bacteria (NOB) convert the nitrite to nitrate. Classical nitrification was considered to be a strictly aerobic process represented by the following bioreactions:

$$\mathrm{NH_4^+} + \tfrac{3}{2}\mathrm{O_2} \xrightarrow{S} \mathrm{NO_2^-}\ (+\mathrm{H_2O} + 2\mathrm{H^+}), \tag{2.1a}$$

$$\mathrm{NO_2^-} + \tfrac{1}{2}\mathrm{O_2} \xrightarrow{B} \mathrm{NO_3^-}. \tag{2.1b}$$

Here, S represents the ammonium-oxidising bacteria, *Nitrosomonas*, while B represents the nitrite-oxidising bacteria *Nitrobacter*. Each of these are commonly found in soil environments[1] (Koops and Pommerening-Röser 2001; Sliekers et al. 2005). Overall, the reactions Eqs. 2.1a and 2.1b sum to the net reaction

$$\mathrm{NH_4^+} + 2\mathrm{O_2} \rightarrow \mathrm{NO_3^-} + \mathrm{H_2O} + 2\mathrm{H^+}. \tag{2.2}$$

Prior to the late twentieth century, there was no conclusive evidence of anaerobic ammonium oxidation and it was generally believed to be a purely aerobic process. However, this conclusion was experimentally shown to be incorrect by Mulder et al. (1995) with the discovery of an anaerobic ammonium oxidation (anammox) process which used nitrite as a terminal electron acceptor. One possible reaction pathway for the anammox process Van der Heijden et al. (1994) and Strous et al. (1998) was posited based on biomass measurement and stoichiometry[2] to be

$$\mathrm{NH_4^+} + \tfrac{33}{25}\mathrm{NO_2^-} + \tfrac{33}{500}\mathrm{HCO_3^-} + \tfrac{13}{100}\mathrm{H^+} \xrightarrow{X} \tfrac{13}{50}\mathrm{NO_3^-} + \tfrac{51}{50}\mathrm{N_2} + \tfrac{33}{500}\mathrm{X} + \tfrac{203}{100}\mathrm{H_2O}, \tag{2.3}$$

where X, chemical formula $\mathrm{CH_2O_{0.5}N_{0.15}}$, represents an anammox bacterial (XOB) biomass with one such species being *Brocadia anammoxidans*. However, it was later discovered that anaerobic ammonium oxidation is not limited solely to the anammox process and can actually be carried out by aerobic ammonium-oxidising bacteria as is evidenced in Fig. 3 where the typically aerobic *Nitrosomonas* bacteria continue to flourish once the oxygen has been removed. Indeed, it was shown by Schmidt and Bock (1997) that AOB such as *Nitrosomonas* can utilise nitrogen dioxide, $\mathrm{NO_2}$, in place of oxygen. In an anoxic environment, the ammonium oxidation equation becomes (Schmidt and Bock 1997, 1998; Schmidt et al. 2001b)

$$\mathrm{NH_4^+} + 2\mathrm{NO_2} \xrightarrow{S} 2\mathrm{NO} + \tfrac{1}{3}\mathrm{NO_2^-} + \tfrac{4}{3}\mathrm{H^+} + \tfrac{1}{3}\mathrm{N_2} + \tfrac{4}{3}\mathrm{H_2O}. \tag{2.4}$$

The borehole data presented in Figs. 1 and 2a does not include any measure for this proposed $\mathrm{NO_2}$ gas pathway and therefore its inclusion may appear unjustified. However, the bacterial community data in Fig. 3 clearly shows a well-sustained population of AOB far beyond the aerobic regime and therefore, some secondary anaerobic reaction must allow the AOB to survive. Chemostat studies of Sliekers et al. (2005) show an increase in nitrous oxide production, a by-product of reaction (2.4), when oxygen limitation is present. As such, we include the $\mathrm{NO_2}$ pathway as a representative suggestion due to the experimental evidence of its inclusion but will clarify the effects of this assumption in the model as the equations are introduced.

The reactions as currently proposed admit a global accumulation of nitrate and any observed oscillations will have a general upward trend. To observe periodic spikes such as those seen in Fig. 1, we will include a simple linear nitrate removal term. This represents nitrate fixation processes, the most common of which is denitrification. Denitrification is the conversion of nitrate into nitrogen gas and is generally performed by facultative anaerobes and anaerobic heterotrophs (Strohm et al. 2007). The former are bacteria that prefer oxygen as a terminal electron acceptor but will utilise other substrates if necessary while the latter rely on complex carbon. However, aerobic nitrifiers have been known to perform denitrification as well (Wrage et al. 2001) and therefore this is not an exclusively anaerobic process.

We anticipate that the nitrification process alone is sufficient to obtain oscillatory behaviour in the borehole data and a proper description of denitrification would only impact factors such as the nutrient amplitude. Since the complexity of nitrate fixation is on a similar scale to denitrification, modelling the entire process would further complicate the model without drastically enhancing the conclusions. Furthermore, as carbon plays a significant role in the denitrification process, a proper model of denitrification should include carbon dynamics of which very little data is available for the borehole under consideration. A numerical model of denitrification presented by Kinzelbach et al. (1991) concluded that carbon sources from both groundwater recharge and organic material affixed to the soil matrix were required to reproduce concentration profiles. Some carbon data is available in Fig. 1 but does not seem to have a high variation of the same magnitude of nitrate and only appears to have interesting dynamics far into the anaerobic regime where it oscillates with ammonium. A model for this long-time

[1] As the Rexco boreholes exist approximately 20 m below the ground, the composition of ground material is mostly sandstone (Broholm et al. 1998) and not the standard, organic rich, material in the first several metres which the term *soil* refers to. Nevertheless, we will use this terminology throughout.

[2] The stoichiometric balance in Eq. 2.3 is not completely resolved. Strous et al. (1998) indicates that certain trace compounds have been omitted from the formula. Furthermore, the equation is based on an extrapolation of data over a series of time steps. Each of these could explain the small stoichiometric errors.

oscillatory behaviour has previously been considered by Fowler et al. (2014).

One of the key assumptions we make in our model is the importance of the biological mediation in the aforementioned chemical processes, that is we assume that the reaction rates depend on the bacterial populations and that the growth of these populations themselves is affected by the chemical reactions. We denote the chemical concentrations as

$$\begin{aligned} &C_{\mathrm{NH_4}} = [\mathrm{NH_4^+}], \quad C_{\mathrm{O_2}} = [\mathrm{O_2}], \quad C_{\mathrm{NO_2}} = [\mathrm{NO_2^-}], \\ &C_{\mathrm{NO_3}} = [\mathrm{NO_3^-}], \quad C_{\mathrm{NO_{2g}}} = [\mathrm{NO_2}], \end{aligned} \tag{2.5}$$

and the bacterial concentrations of *Nitrosomonas*, *Nitrobacter*, and *B. anammoxidans* as C_{AOB}, C_{NOB}, and C_{XOB} respectively where each concentration has units mg L^{-1}. We ignore the chemical species which do not carry forward to other nitrification reactions for simplicity. Focusing only on these components, we rewrite the chemical reactions (2.1a), (2.1b), (2.3), and (2.4) as

$$\begin{aligned} &C_{\mathrm{NH_4}} + \tfrac{3}{2}C_{\mathrm{O_2}} \overset{C_{\mathrm{AOB}}}{\rightarrow} C_{\mathrm{NO_2}}, \\ &C_{\mathrm{NO_2}} + \tfrac{1}{2}C_{\mathrm{O_2}} \overset{C_{\mathrm{NOB}}}{\rightarrow} C_{\mathrm{NO_3}}, \\ &C_{\mathrm{NH_4}} + \tfrac{33}{25}C_{\mathrm{NO_2}} \overset{C_{\mathrm{XOB}}}{\rightarrow} \tfrac{13}{50}C_{\mathrm{NO_3}}, \\ &C_{\mathrm{NH_4}} + 2C_{\mathrm{NO_{2g}}} \overset{C_{\mathrm{AOB}}}{\rightarrow} \tfrac{1}{3}C_{\mathrm{NO_2}}, \end{aligned} \tag{2.6}$$

and then pose rate equations using standard mass action kinetics as

$$\begin{aligned} \dot{C}_{\mathrm{NO_2}} &= \tfrac{1}{Y_S}r_{S1} - \tfrac{1}{Y_B}r_B + \tfrac{1}{3}\tfrac{1}{Y_S}r_{S2} - \tfrac{33}{25}\tfrac{1}{Y_X}r_X, \\ \dot{C}_{\mathrm{O_2}} &= I_O - \tfrac{3}{2}\tfrac{1}{Y_S}r_{S1} - \tfrac{1}{2}\tfrac{1}{Y_B}r_B, \\ \dot{C}_{\mathrm{NH_4}} &= I_A - \tfrac{1}{Y_S}r_{S2} - \tfrac{1}{Y_X}r_X - \tfrac{1}{Y_S}r_{S1} \\ &\quad +\zeta\left(\tfrac{d_S}{Y_S}C_{\mathrm{AOB}} + \tfrac{d_B}{Y_B}C_{\mathrm{NOB}} + \tfrac{d_X}{Y_X}C_{\mathrm{XOB}}\right), \\ \dot{C}_{\mathrm{NO_3}} &= \tfrac{1}{Y_B}r_B + \tfrac{13}{50}\tfrac{1}{Y_X}r_X - e_P C_{\mathrm{NO_3}}, \\ \dot{C}_{\mathrm{AOB}} &= r_{S1} + r_{S2} - d_S C_{\mathrm{AOB}}, \\ \dot{C}_{\mathrm{NOB}} &= r_B - d_B C_{\mathrm{NOB}}, \\ \dot{C}_{\mathrm{XOB}} &= r_X - d_X C_{\mathrm{XOB}}. \end{aligned} \tag{2.7}$$

The reaction rates are taken to be of Monod type following (Monod 1949) and satisfy

$$\begin{aligned} r_{S1} &= \mu_S \tfrac{C_{\mathrm{NH_4}}C_{\mathrm{O_2}}C_{\mathrm{AOB}}}{(C_{\mathrm{NH_4}}+k_{AS})(C_{\mathrm{O_2}}+k_{GS})}, \\ r_{S2} &= \mu_S \tfrac{C_{\mathrm{NH_4}}C_{\mathrm{NO_{2g}}}C_{\mathrm{AOB}}}{(C_{\mathrm{NH_4}}+k_{AS})(C_{\mathrm{NO_{2g}}}+k_{MS})}H, \\ r_B &= \mu_B \tfrac{C_{\mathrm{NO_2}}C_{\mathrm{O_2}}C_{\mathrm{NOB}}}{(C_{\mathrm{NO_2}}+k_{NB})(C_{\mathrm{O_2}}+k_{GB})}, \\ r_X &= \mu_X \tfrac{C_{\mathrm{NO_2}}C_{\mathrm{NH_4}}C_{\mathrm{XOB}}}{(C_{\mathrm{NO_2}}+k_{NX})(C_{\mathrm{NH_4}}+k_{AX})}H, \end{aligned} \tag{2.8}$$

where H, given by

$$H = \frac{k_I}{k_I + C_{\mathrm{O_2}}}, \tag{2.9}$$

represents the inhibition for anaerobic processes to oxygen. The Monod terms act in the same way as Michaelis-Menton kinetics of Michaelis and Menten (1913) for enzyme bonding. These types of kinetics are generally used for microbially mediated transformations such as in Maggi et al. (2008) and represent the metabolic limits that bacteria have in the presence of high nutrient supply. If nutrient concentrations are very small, then the reaction rates become first-order linear mass action kinetics and when very large, they reduce to zeroth-order kinetics at a maximal rate. The abstract nutrient model in Huisman and Weissing (1999) also uses Monod kinetics but rather than multiply each Monod term involved in a reaction, they take the minimum under assumption that this limits the reaction. We maintain a general formulation for our reaction and allow the scaling to dictate limiting mechanics and whether reductions to first or zeroth order kinetics are appropriate. The inhibition term (2.9) is a decreasing function which has a maximum value of one if the oxygen concentration is zero (supports anaerobic growth) and tends to zero (inhibits anaerobic growth) as the concentration gets large.

There are also non-microbially mediated nutrient transformation processes such as aqueous complexation, gas dissolution, and adsorption. The first two are ignored on the basis that nitrification is not a spontaneous chemical transformation and requires bacterial involvement. This is most evidenced by Figs. 2 and 3 where spikes in nitrate correspond to spikes in bacterial population. Considering only the nutrients in our model, Mekala et al. (2017) states that ammonium is the most dominant for adsorption. If we consider including adsorption of ammonium to some particulate phase with concentration $C_{\mathrm{NH_{4s}}}$, then the ammonium model would transform to

$$\begin{aligned} \dot{C}_{\mathrm{NH_4}} &= \quad R - \kappa_A C_{\mathrm{NH_4}} + \kappa_D C_{\mathrm{NH_{4s}}}, \\ \tau\dot{C}_{\mathrm{NH_{4s}}} &= \kappa_A C_{\mathrm{NH_4}} + \kappa_D C_{\mathrm{NH_{4s}}}, \end{aligned} \tag{2.10}$$

where κ_A and κ_D are the adsorption and desorption coefficients, respectively, R represents the reactions already considered in Eq. 2.7_3, and τ is the time scale of adsorption equilibrium for the particulate and mobile phases. Typically, following for example Fowler (2011), this time scale is small and the particulate and mobile phases quickly reach equilibrium, $C_{\mathrm{NH_{4s}}} = \frac{\kappa_A}{\kappa_D}C_{\mathrm{NH_4}}$, and the particulate phase can be removed by adding the equations

$$\left(1 + \frac{\tau\kappa_A}{\kappa_D}\right)\dot{C}_{\mathrm{NH_4}} = R. \tag{2.11}$$

We recover the ammonium model $(2.7)_3$ with a modified time scale $\left(1 + \frac{\tau\kappa_A}{\kappa_D}\right)$ which affects the organic rates of reaction. We ignore this scaling on the assumption that $\frac{\tau\kappa_A}{\kappa_D}$ is very small and therefore the adjustments are negligible. Furthermore, Yu et al. (2011) and Ranjbar and Jalali (2013) state that ammonium adsorption is comparable to nitrate leeching in terms of nitrogen losses and we do not model leeching so it seems appropriate to also discount adsorption as well.

The coefficients Y_i in Eq. 2.7 are yield coefficients, d_i are death rates, μ_i are the maximal bacterial activity, k_{ij} are the saturation constants for bacteria j feeding on nutrient i, e_P is the nitrate removal rate, k_I the oxygen inhibition concentration, and ζ is a dimensionless recycling coefficient. The source terms I_O and I_A represent inputs of oxygen and ammonium respectively and are necessary in a chemostat situation where batch reactors are used to grow bacterial cultures. In a more physical groundwater situation, oxygen is supplied by diffusion from the oxygenated surface water and therefore an input seems rather inappropriate in that model. However, regarding ammonium, a common soil process is ammonification which is the recycling of ammonium due to bacterial predation and conversion of natural soil organic material (Barber 1995), the latter of which is likely insignificant due to the depths considered. While some of the soil ammonification is captured by the recycling term multiplying ζ in Eq. 2.7_3, there are many more bacterial and fungal species not being modelled which would have a large contribution on ammonium recycling. Therefore, in the interest of a simplified model, ammonification will be captured by allowing the source term I_A to remain in a full soil borehole model.

Since no data is available on NO_2 gas in the borehole, we will take it to be a constant, the consequence of which is that Eq. 2.7 becomes a closed system. We will further assume that NO_2 is in abundant supply for the bacteria, i.e. that $C_{NO_{2g}} \gg k_{MS}$ so that

$$\bar{C}_{NO_{2g}} = \frac{C_{NO_{2g}}}{C_{NO_{2g}} + k_{MS}} \approx 1. \tag{2.12}$$

Using this assumption allows for any nutrient to be used in place of NO_2 as long as it is not rate limiting the growth of AOB and its inclusion merely allows for an anaerobic transformation of ammonium to nitrite.

Model parameters and non-dimensionalisation

There are two approaches one can take when attempting a parameter estimation for Eq. 2.7. The first approach is to use the data in Fig. 2 which provides an approximate nutrient scale for each of the components for the particular borehole. These scalings could be applied to the model and used to infer parameter estimates for the Monod reactions. Alternatively, values for each of the kinetic parameters used could be obtained from experiments found in literature and nutrient scales would follow. Ideally, both approaches would be consistent and produce similar estimates but the high degree of system complexity mixed with strong variation between lab- and field-scale parameters means this will generally not be true. For example, Charoanwoodtipong et al. (2015) showed that specific nutrient parameters can be very sensitive to the ambient levels of nutrient itself, intimately connecting parameter and nutrient scale. However, a mathematical model should be reasonably robust to parameter estimation error if it is to ever capture and explain the observed behaviour.

We will use the method of taking experimental parameter values for scales as this approach has a more intimate connection to the model choice compared to selecting scales from the data. There is no experimental parameter for I_A or I_O as these are model-specific parameters. We will fix the ammonium input as this is relevant to both a chemostat and soil situation and then allow their ratio $\beta = I_O/I_A$ to vary with the caveat that $\beta = 0$ in the soil problem.

Since we anticipate that the ammonification rate is tied to bacterial recycling then it is natural to choose I_A as a bacterial scale multiplied by an anaerobic environment decay rate. A study by Whitman et al. (1998) details the carbon content of prokaryotic cells on Earth noting that soil bacteria cumulatively contain approximately 26×10^{18} mgC and offer a C:N ratio of 8.6 leading to 3.02×10^{18} mgN. They further state that soil environments support approximately 26×10^{28} bacterial cells while Alfreider et al. (1997) measure that sandy environments have approximately 52×10^9 cells L^{-1}. Combining this information gives a bacterial nitrogen content of approximately 0.6 mg L^{-1}. Salem et al. (2006) reports that in anaerobic conditions, bacterial decay rates are on the order of 10^{-2} day^{-1}. Multiplying these numbers together, we will take $I_A = 6 \times 10^{-3}$ mg L^{-1} d^{-1}. Furthermore, we will consider $\zeta = 0$ so that I_A captures all the ammonium recycling. Since we have simplified the model of denitrification to a linear proportionality to C_{NO_3}, there is no clear mechanism for choosing the denitrification rate e_P. Instead, we will choose this through a convenient choice of a non-dimensional parameter. Model parameters are presented in Table 1.

By observation in Fig. 2, the interesting spatial dynamics appear in the anoxic regime and so we will non-dimensionalise (2.7) using scales appropriate to that region:

$$\begin{aligned}
&C_{NH_4} \sim C^0_{NH_4} \equiv \frac{d_S k_{AS}}{\mu_S}, && C_{NO_2} \sim C^0_{NO_2} \equiv \tfrac{d_X k_{NX}}{\mu_X}, && C_{NO_3} \sim C^0_{NO_3} \equiv C^0_{NH_4},\\
&C_{AOB} \sim C^0_{AOB} \equiv \frac{I_A Y_S}{d_S}, && C_{XOB} \sim C^0_{XOB} \equiv \tfrac{I_A Y_X}{d_X}, && C_{NOB} \sim C^0_{NOB} \equiv \tfrac{I_A Y_B}{d_B},\\
&C_{O_2} \sim C^0_{O_2} \equiv \frac{\mu_X d_B k_{NB} k_{GB}}{\mu_B d_X k_{NX}}, && t \sim t_0 \equiv \sqrt{\tfrac{k_{AS}}{\mu_S I_A}},
\end{aligned} \tag{2.13}$$

and the dimensionless equations become (with the dimensionless variables in lower case and η being the dimensionless H)

$$
\begin{aligned}
\dot{c}_{\mathrm{NO_2}} &= \epsilon\gamma_N\left[\frac{c_{\mathrm{NH_4}}c_{\mathrm{O_2}}c_{\mathrm{AOB}}}{(\omega_{AS}c_{\mathrm{NH_4}}+1)(c_{\mathrm{O_2}}+\Omega_{GS})}-\frac{c_{\mathrm{NO_2}}c_{\mathrm{O_2}}c_{\mathrm{NOB}}}{(\omega_{NB}c_{\mathrm{NO_2}}+1)(\omega_{GB}c_{\mathrm{O_2}}+1)}\right.\\
&\quad\left.+\frac{1}{3}\frac{c_{\mathrm{NH_4}}c_{\mathrm{AOB}}}{(\omega_{AS}c_{\mathrm{NH_4}}+1)}\eta-\frac{33}{25}\frac{c_{\mathrm{NO_2}}c_{\mathrm{NH_4}}c_{\mathrm{XOB}}}{(c_{\mathrm{NH_4}}+\Omega_{AX})(\omega_{NX}c_{\mathrm{NO_2}}+1)}\eta\right],\\
\dot{c}_{\mathrm{O_2}} &= \epsilon\gamma_G\left[\beta-\frac{3}{2}\frac{c_{\mathrm{NH_4}}c_{\mathrm{O_2}}c_{\mathrm{AOB}}}{(\omega_{AS}c_{\mathrm{NH_4}}+1)(c_{\mathrm{O_2}}+\Omega_{GS})}-\frac{1}{2}\frac{c_{\mathrm{NO_2}}c_{\mathrm{O_2}}c_{\mathrm{NOB}}}{(\omega_{NB}c_{\mathrm{NO_2}}+1)(\omega_{GB}c_{\mathrm{O_2}}+1)}\right],\\
\dot{c}_{\mathrm{NH_4}} &= \epsilon\left[1-\frac{c_{\mathrm{NH_4}}c_{\mathrm{O_2}}c_{\mathrm{AOB}}}{(\omega_{AS}c_{\mathrm{NH_4}}+1)(c_{\mathrm{O_2}}+\Omega_{GS})}-\frac{c_{\mathrm{NH_4}}c_{\mathrm{AOB}}}{\omega_{AS}c_{\mathrm{NH_4}}+1}\eta-\frac{c_{\mathrm{NO_2}}c_{\mathrm{NH_4}}c_{\mathrm{XOB}}}{(c_{\mathrm{NH_4}}+\Omega_{AX})(\omega_{NX}c_{\mathrm{NO_2}}+1)}\eta\right],\\
\dot{c}_{\mathrm{NO_3}} &= \epsilon\left[\frac{c_{\mathrm{NO_2}}c_{\mathrm{O_2}}c_{\mathrm{NOB}}}{(\omega_{NB}c_{\mathrm{NO_2}}+1)(\omega_{GB}c_{\mathrm{O_2}}+1)}+\frac{13}{50}\frac{c_{\mathrm{NO_2}}c_{\mathrm{NH_4}}c_{\mathrm{XOB}}}{(c_{\mathrm{NH_4}}+\Omega_{AX})(\omega_{NX}c_{\mathrm{NO_2}}+1)}\eta-c_{\mathrm{NO_3}}\right],\\
\epsilon\dot{c}_{\mathrm{AOB}} &= \frac{c_{\mathrm{NH_4}}c_{\mathrm{O_2}}c_{\mathrm{AOB}}}{(\omega_{AS}c_{\mathrm{NH_4}}+1)(c_{\mathrm{O_2}}+\Omega_{GS})}+\frac{c_{\mathrm{NH_4}}c_{\mathrm{AOB}}}{\omega_{AS}c_{\mathrm{NH_4}}+1}\eta-c_{\mathrm{AOB}},\\
\epsilon\lambda_B\dot{c}_{\mathrm{NOB}} &= \frac{c_{\mathrm{NO_2}}c_{\mathrm{O_2}}c_{\mathrm{NOB}}}{(\omega_{NB}c_{\mathrm{NO_2}}+1)(\omega_{GB}c_{\mathrm{O_2}}+1)}-c_{\mathrm{NOB}},\\
\epsilon\lambda_X\dot{c}_{\mathrm{XOB}} &= \frac{c_{\mathrm{NO_2}}c_{\mathrm{NH_4}}c_{\mathrm{XOB}}}{(c_{\mathrm{NH_4}}+\Omega_{AX})(\omega_{NX}c_{\mathrm{NO_2}}+1)}\eta-c_{\mathrm{XOB}},\\
\eta &= \frac{\kappa}{\kappa+c_{\mathrm{O_2}}},
\end{aligned}
\tag{2.14}
$$

where

$$
\epsilon=\sqrt{\frac{\mu_S I_A}{k_{AS}d_S^2}},\qquad \gamma_J=\frac{C^0_{\mathrm{NH_4}}}{C^0_j},\qquad \lambda_J=\frac{d_S}{d_J},\qquad \beta=\frac{I_O}{I_A},
$$
$$
\kappa=\frac{k_I}{C^0_{\mathrm{O_2}}},\qquad \omega_{ij}=\frac{i^0}{k_{ij}},\qquad \Omega_{ij}=\frac{k_{ij}}{i^0},
\tag{2.15}
$$

and conditions of nutrient starvation are associated with the limit $\epsilon \ll 1$. By writing $(2.14)_4$ and choosing $C^0_{\mathrm{NO_3}} = C^0_{\mathrm{NH_4}}$, we have taken the nitrate removal rate coefficient $e_P = 1.8\times10^{-3}\ \mathrm{d}^{-1}$. Since this is a rate for a simplified process, it is hard to justify its validity; however, it is the same order of magnitude as the recycling rate which is sensible. The choice of $C^0_{\mathrm{NO_3}} = C^0_{\mathrm{NH_4}}$ follows from the similar scales which appear in Fig. 2. All of the scales and dimensionless values are presented in Table 2 using parameter choices from Table 1. The observed values for each nutrient are based on order estimates from data in Fig. 2a, b while the bacterial values follow discussions in "Model parameters and non-dimensionalisation" following calculations from Whitman et al. (1998) and Alfreider et al. (1997). The reaction time scale is a consequence of the model scaling and an observed value is not available in reference literature. It is of interest to note that the scales of bacterial nitrogen content, C^0_{AOB}, C^0_{NOB}, and C^0_{XOB} which are derived using the chosen parameter I_A are consistent with values presented by Kogure and Koike (1987) and also the computed reference value in "Model parameters and non-dimensionalisation".

A full study of the steady states of the highly nonlinear problem (2.14) is beyond the scope of this manuscript and instead we will focus on a strongly anaerobic regime[3] by setting $\beta = 0$. However, numerical investigations of Eq. 2.14 indicate that multiple steady states do exist for $\beta > 0$ and not too large. This indicates a resource competition dependent on oxygen supply. Indeed, this competition has been observed in oxygen-limited reactors where nitrite-oxidising bacteria were not detected (Schmidt et al. 2001b; Helder and De Vries 1983; Hanaki et al. 1990) and it was postulated that ammonium-oxidising bacteria have a stronger affinity for oxygen over NOB while the anammox bacteria have a stronger affinity for nitrite over NOB.

[3] This seems to be in disagreement with the large nitrate spike observed in the aerobic region of Figs. 1 and 2b, but we will resolve this in the full soil problem. We focus on the anaerobic region since the secondary oscillations form here.

Table 1 Model parameters

Symbol	Description	Value	Reference
d_S	Decay rate AOB	0.2 day^{-1}	Salem et al. (2006)
d_B	Decay rate NOB	0.2 day^{-1}	Salem et al. (2006)
d_X	Decay rate XOB	4.8×10^{-3} day^{-1}	Scaglione et al. (2009)
μ_S	Maximum activity AOB	0.8 day^{-1}	Munz et al. (2011)
μ_B	Maximum activity NOB	1.11 day^{-1}	Munz et al. (2011)
μ_X	Maximum activity XOB	0.1 day^{-1}	Oshiki et al. (2011)
k_{AS}	NH_4^+ half-saturation constant AOB	11.18 mg L^{-1}	Sliekers et al. (2005)
k_{GS}	O_2 half-saturation constant AOB	0.6 mg L^{-1}	Wiesmann (1994)
k_{NB}	NO_2^- half-saturation constant NOB	2.25 mg L^{-1}	Nowka et al. (2015)
k_{GB}	O_2 half-saturation constant NOB	2.2 mg L^{-1}	Wiesmann (1994)
k_{AX}	NH_4^+ half-saturation constant XOB	0.5 mg L^{-1}	Oshiki et al. (2011)
k_{NX}	NO_2^- half-saturation constant XOB	3.96 mg L^{-1}	Oshiki et al. (2011)
Y_S	Yield coefficient AOB	0.14	Blackburne et al. (2007)
Y_B	Yield coefficient NOB	0.1	Nowka et al. (2015)
Y_X	Yield coefficient XOB	0.159	Strous et al. (1998)
k_I	O_2 inhibition coefficient	0.07 mg L^{-1}	Schmidt et al. (2001b)
I_A	NH_4^+ input/ammonification	6×10^{-3} mg $\text{L}^{-1}\text{d}^{-1}$	Chosen
e_P	Denitrification rate	1.8×10^{-3} day^{-1}	Chosen

A reduced anaerobic system

Taking $\beta = 0$ in Eq. 2.14 results in $c_{\text{O}_2} = c_{\text{NOB}} = 0$ as steady-state oxygen and *Nitrobacter* values respectively and we get a reduced anaerobic system,

$$\begin{aligned}
\dot{c}_{\text{NO}_2} &= \epsilon\gamma_N\left(\tfrac{1}{3}c_{\text{NH}_4}c_{\text{AOB}} - \tfrac{33}{25}c_{\text{NO}_2}c_{\text{XOB}}\right),\\
\dot{c}_{\text{NH}_4} &= \epsilon\left(1 - c_{\text{NH}_4}c_{\text{AOB}} - c_{\text{NO}_2}c_{\text{XOB}}\right),\\
\dot{c}_{\text{NO}_3} &= \epsilon\left(\tfrac{13}{50}c_{\text{NO}_2}c_{\text{XOB}} - c_{\text{NO}_3}\right),\\
\epsilon\dot{c}_{\text{AOB}} &= c_{\text{AOB}}(c_{\text{NH}_4} - 1),\\
\epsilon\lambda_X\dot{c}_{\text{XOB}} &= c_{\text{XOB}}(c_{\text{NO}_2} - 1),
\end{aligned} \tag{2.16}$$

where we have taken $\omega_{ij} = \Omega_{ij} = 0$ on the basis that they are small and $\eta = 1$ since $c_{\text{O}_2} = 0$. We are predominantly interested in this anaerobic problem because the spatial inhomogeneity in Fig. 2 appears to come from this regime. The reduced model (2.16) has the steady state[4] $[c_{\text{NO}_2}, c_{\text{NH}_4}, c_{\text{NO}_3}, c_{\text{AOB}}, c_{\text{XOB}}] = \left[1, 1, \frac{13}{248}, \frac{99}{124}, \frac{25}{124}\right]$ and is conveniently simplified by writing

$$c_{\text{AOB}} = \tfrac{99}{124}\text{e}^{\theta}, \quad c_{\text{XOB}} = \tfrac{25}{124}\text{e}^{\phi}; \tag{2.17}$$

which results in the coupled oscillator pair (ignoring the decoupled nitrate problem)

$$\begin{aligned}
\ddot{\theta} &= 1 - \tfrac{99}{124}(1+\epsilon\dot{\theta})\text{e}^{\theta} - \tfrac{25}{124}(1+\epsilon\lambda_X\dot{\phi})\text{e}^{\phi},\\
\lambda_X\ddot{\phi} &= \tfrac{33}{124}\gamma_N\left((1+\epsilon\dot{\theta})\text{e}^{\theta} - (1+\epsilon\lambda_X\dot{\phi})\text{e}^{\phi}\right),
\end{aligned} \tag{2.18}$$

with steady state $\theta = \phi = 0$. In Appendix A, we perform a linear stability analysis around this steady state, the conclusion of which is that the constant state is oscillatorily unstable provided $\lambda > 1$ and that γ_N falls into the weak instability band[5]

$$\begin{aligned}
&\bar{\gamma}_N^- < \gamma_N < \bar{\gamma}_N^+;\\
&\bar{\gamma}_N^{\pm}\tfrac{25}{66}\left(\lambda_X^2 + \tfrac{248}{25}\lambda_X + 1 \pm \tfrac{(\lambda_X+1)}{5}\sqrt{25\lambda_X^2 + 446\lambda_X + 25}\right).
\end{aligned} \tag{2.19}$$

Using Table 2, we calculate $\bar{\gamma_N}^- = 9.65$ and $\bar{\gamma}_N^+ = 1.62\times10^3$ and γ_N falls into this threshold. Therefore, for simulations of $[c_{\text{NO}_2}, c_{\text{NH}_4}, c_{\text{NO}_3}, c_{\text{AOB}}, c_{\text{XOB}}]$ near the base state, we should anticipate periodic solutions to emerge.

Results

Temporal oscillations

To illustrate the presence of oscillatory solutions, we simulate (2.16) acknowledging that the choice of parameters in Table 1, specifically $\lambda_X = 41.67$ and $\gamma_N = 14.7$, falls within the weak instability band (2.19). We perform the simulations in MATLAB using the differential equation solver `ode45`, the results of which are in Fig. 4 for the chosen non-dimensional window $t = 900$ to $t = 1000$.

It can be seen that the solutions are periodic and are similar to the spike-like oscillations found in related systems

[4] If ζ were non-zero, then this only serves to modify these steady-state values.

[5] See Appendix A for a discussion of what is meant by a weak instability band.

Table 2 Dimensional scales and parameter values

Symbol	Value	Observed Value
$C^0_{NH_4}$	2.8 mg L^{-1}	100 mg L^{-1}
$C^0_{NO_2}$	0.19 mg L^{-1}	4 mg L^{-1}
$C^0_{O_2}$	4.7 mg L^{-1}	6 mg L^{-1}
$C^0_{NO_3}$	2.8 mg L^{-1}	100 mg L^{-1}
C^0_{AOB}	4.2×10^{-3} mg L^{-1}	0.6 mg L^{-1}
C^0_{NOB}	3.0×10^{-3} mg L^{-1}	0.6 mg L^{-1}
C^0_{XOB}	0.2 mg L^{-1}	0.6 mg L^{-1}
t_0	58.3 d	—
ϵ	0.1	
γ_N	14.70	
γ_G	0.6	
λ_B	1	
λ_X	41.7	
κ	0.015	
ω_{AS}	0.25	
Ω_{GS}	0.13	
ω_{NB}	0.08	
ω_{GB}	2.13	
Ω_{AX}	0.18	
ω_{NX}	0.048	

by Fowler (2014) and Fowler et al. (2014), as well as other models such as Huisman and Weissing (1999) and Maggi et al. (2008). In particular, both bacterial populations exhibit boom-and-bust dynamics, with short-lived outbreaks followed by long quiescent intervals, while the principal nutrients, ammonium and nitrite, recover. The spiky nature of the oscillations is associated with small values of ϵ. The nitrate production (Fig. 4e) is essentially inverse to the ammonium cycling, and this can be understood since the overall resource flow is ammonium to nitrate, and when ϵ is small, the model (2.16) somewhat resembles that of Michaelis-Menten kinetics, with the bacterial populations playing the role of enzymes. In Fig. 5, we plot the dimensional C_{AOB} and C_{XOB} bacteria using the scales in Table 2 to show the out-of-phase oscillations that they exhibit. This phase shift is also observed in the data of Fig. 3.

Spatial oscillations

We now seek to model a more realistic borehole profile where spatial nutrient transport is permitted. There are two transport mechanisms: advection by groundwater flow, and diffusion or dispersion. Longitudinal dispersion is generally $\sim d_p U$, where d_p is the pore diameter and U is the groundwater velocity, if the pore-scale Péclet number is large (i. e. $d_p U \gg D$, where D is the diffusion coefficient). In the present case, this is unlikely to be the case, and the dispersion coefficient is just D. The magnitude of the horizontal advection term is given by the reduced Péclet number, which is

$$\mathrm{Pe} = \frac{U l_v^2}{D l_h}, \tag{3.1}$$

where l_v and l_h are the vertical and horizontal length scales. Typically, this is large so that advection dominates the transport equation. However, when the groundwater flow is spatially uniform, as is realistic here, the advective derivative can be replaced by a (Lagrangian) time derivative which describes the evolution of the chemical components of the groundwater column as it moves, and the only effective transport in the column is through vertical diffusion. This simplification is enabled by the fact that $l_v \ll l_h$, so that horizontal transport between neighbouring columns can be neglected.

It is known (see Fowler (2011) and Kopell and Howard (1973)) that when a temporal system exhibits periodic kinetics, the addition of spatial diffusion can induce wave trains. A similar strategy was used for carbon cycling in McGuinness et al. (2014), where travelling waves were indeed observed. However, in that analysis, the reaction was assumed to begin in the centre of an infinite medium and propagate outwards. Instead, we seek to modify the spatially independent system (2.14) to include oxygen supply from a phreatic interface rather than as a volumetric source term. However, as previously discussed, it is natural to leave the volumetric source of ammonium to simulate the recharge

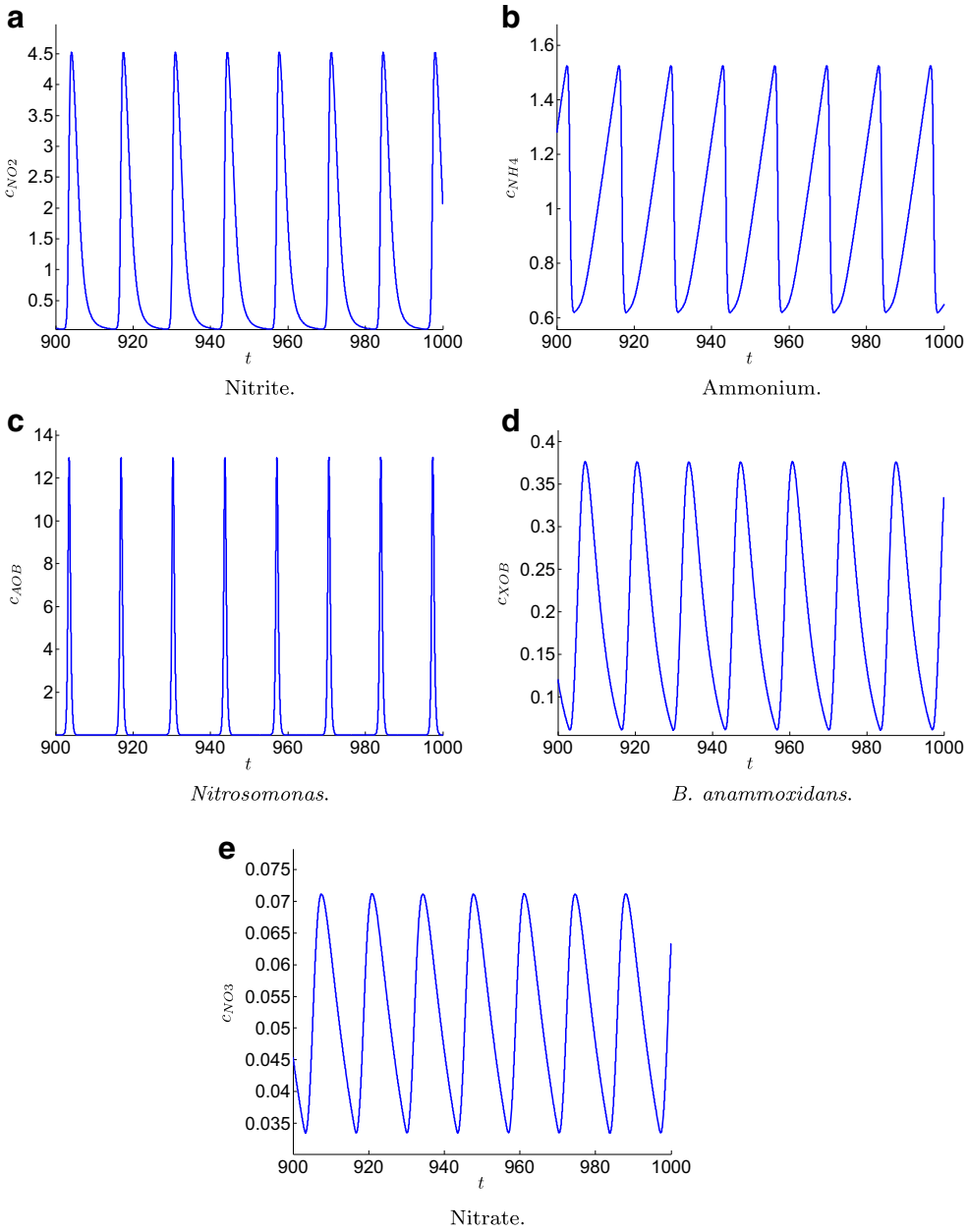

Fig. 4 Solutions of (2.16) with the parameter set $\lambda_X = 41.67$, $\gamma_N = 14.7$, $\epsilon = 0.1$, and $\gamma_P = 1$. Solutions plotted are for **a** Nitrite, **b** Ammonium, **c** Nitrosomonas, **d** B. anammoxidans, and **e** nitrate

due to microbial recycling. We introduce a space dimension $z \in [0, \infty)$ to represent the depth of the soil with $z = 0$ being the depth of the water table (15 m in Fig. 2) and downward is positive. Introducing diffusion transforms (2.7) to

$$\begin{aligned}
C_{\mathrm{NO}_2 t} &= \tfrac{1}{Y_S} r_{S1} - \tfrac{1}{Y_B} r_B + \tfrac{1}{3}\tfrac{1}{Y_S} r_{S2} - \tfrac{33}{25}\tfrac{1}{Y_X} r_X + D_N C_{\mathrm{NO}_2 zz},\\
C_{\mathrm{O}_2 t} &= -\tfrac{3}{2}\tfrac{1}{Y_S} r_{S1} - \tfrac{1}{2}\tfrac{1}{Y_B} r_B + D_G C_{\mathrm{O}_2 zz},\\
C_{\mathrm{NH}_4 t} &= I_A - \tfrac{1}{Y_S} r_{S2} - \tfrac{1}{Y_X} r_X - \tfrac{1}{Y_S} r_{S1} + D_A C_{\mathrm{NH}_4 zz},\\
C_{\mathrm{NO}_3 t} &= \tfrac{1}{Y_B} r_B + \tfrac{13}{50}\tfrac{1}{Y_X} r_X - e_p P + D_P C_{\mathrm{NO}_3 zz},\\
C_{\mathrm{AOB}_t} &= r_{S1} + r_{S2} - d_S C_{\mathrm{AOB}},\\
C_{\mathrm{NOB}t} &= r_B - d_B C_{\mathrm{NOB}},\\
C_{\mathrm{XOB}t} &= r_X - d_X C_{\mathrm{XOB}},
\end{aligned} \tag{3.2}$$

where the subscripts z and t denote space and time partial derivatives respectively, D_J are diffusion coefficients, and r_{S1}, r_{S2}, r_B, and r_X are given by Eq. 2.8. Note that we have once again taken $\zeta = 0$ allowing I_A to represent ammonification and $I_O = 0$ to reflect the absence of the oxygen volumetric source term. We supplement this with boundary conditions that the far-field flux of each nutrient must vanish and that there is no nutrient present at the phreatic surface aside from oxygen where we instead specify a concentration $C_{\mathrm{O}_2}(0, t) = \bar{C}_{\mathrm{O}_2} = 9.6$ mg L^{-1} due to solubility from atmospheric oxygen[6]. The zero

[6]The computation of $\bar{C}_{\mathrm{O}_2}$ comes from using Henry's Law with a typical atmospheric oxygen pressure of 0.23 atm and a Henry's Law constant of 1.3×10^{-3} mol atm^{-1} L^{-1} from Sander (2015).

condition for the other nutrients is motivated by the plume formation away from the water table and the recharge of fresh water without nutrients due to rainfall. We initialise each bacterial population with a small but finite value to avoid an extinct initial state and we consider zero initial conditions for all nutrients except for ammonium where we take half the observed value (50 mg L^{-1}). We choose half the observed value to compensate for the dynamic production of ammonium through ammonification.

Non-dimensionalising (3.2), we maintain the scalings (2.13) and introduce the scale $z \sim L$ for some typical vertical length scale which we take to be 1 m, consistent with the length scale in Fig. 2. This results in the non-dimensional spatial model

$$
\begin{aligned}
c_{\mathrm{NO}_2 t} &= \epsilon\gamma_N \left[\frac{c_{\mathrm{NH}_4} c_{\mathrm{O}_2} c_{\mathrm{AOB}}}{(\omega_{AS} c_{\mathrm{NH}_4} + 1)(c_{\mathrm{O}_2} + \Omega_{GS})} - \frac{c_{\mathrm{NO}_2} c_{\mathrm{O}_2} c_{\mathrm{NOB}}}{(\omega_{NB} c_{\mathrm{NO}_2} + 1)(\omega_{GB} c_{\mathrm{O}_2} + 1)} \right. \\
&\quad \left. + \frac{1}{3} \frac{c_{\mathrm{NH}_4} c_{\mathrm{AOB}}}{(\omega_{AS} c_{\mathrm{NH}_4} + 1)} \eta - \frac{33}{25} \frac{c_{\mathrm{NO}_2} c_{\mathrm{NH}_4} c_{\mathrm{XOB}}}{(c_{\mathrm{NH}_4} + \Omega_{AX})(\omega_{NX} c_{\mathrm{NO}_2} + 1)} \eta \right] + \nu \delta_N c_{\mathrm{NO}_2 zz}, \\
c_{\mathrm{O}_2 t} &= \epsilon\gamma_G \left[-\frac{3}{2} \frac{c_{\mathrm{NH}_4} c_{\mathrm{O}_2} c_{\mathrm{AOB}}}{(\omega_{AS} c_{\mathrm{NH}_4} + 1)(c_{\mathrm{O}_2} + \Omega_{GS})} - \frac{1}{2} \frac{c_{\mathrm{NO}_2} c_{\mathrm{O}_2} c_{\mathrm{NOB}}}{(\omega_{NB} c_{\mathrm{NO}_2} + 1)(\omega_{GB} c_{\mathrm{O}_2} + 1)} \right] + \nu c_{\mathrm{O}_2 zz}, \\
c_{\mathrm{NH}_4 t} &= \epsilon \left[1 - \frac{c_{\mathrm{NH}_4} c_{\mathrm{O}_2} c_{\mathrm{AOB}}}{(\omega_{AS} c_{\mathrm{NH}_4} + 1)(c_{\mathrm{O}_2} + \Omega_{GS})} - \frac{c_{\mathrm{NH}_4} c_{\mathrm{AOB}}}{\omega_{AS} c_{\mathrm{NH}_4} + 1} \eta \right. \\
&\quad \left. - \frac{c_{\mathrm{NO}_2} c_{\mathrm{NH}_4} c_{\mathrm{XOB}}}{(c_{\mathrm{NH}_4} + \Omega_{AX})(\omega_{NX} c_{\mathrm{NO}_2} + 1)} \eta \right] + \nu \delta_A c_{\mathrm{NH}_4 zz}, \\
c_{\mathrm{NO}_3 t} &= \epsilon \left[\frac{c_{\mathrm{NO}_2} c_{\mathrm{O}_2} c_{\mathrm{NOB}}}{(\omega_{NB} c_{\mathrm{NO}_2} + 1)(\omega_{GB} c_{\mathrm{O}_2} + 1)} + \frac{13}{50} \frac{c_{\mathrm{NO}_2} c_{\mathrm{NH}_4} c_{\mathrm{XOB}}}{(c_{\mathrm{NH}_4} + \Omega_{AX})(\omega_{NX} c_{\mathrm{NO}_2} + 1)} \eta - c_{\mathrm{NO}_3} \right] \\
&\quad + \nu \delta_P c_{\mathrm{NO}_3 zz}, \\
\epsilon c_{\mathrm{AOB}t} &= \frac{c_{\mathrm{NH}_4} c_{\mathrm{O}_2} c_{\mathrm{AOB}}}{(\omega_{AS} c_{\mathrm{NH}_4} + 1)(c_{\mathrm{O}_2} + \Omega_{GS})} + \frac{c_{\mathrm{NH}_4} c_{\mathrm{AOB}}}{\omega_{AS} c_{\mathrm{NH}_4} + 1} \eta - c_{\mathrm{AOB}}, \\
\epsilon\lambda_B c_{\mathrm{NOB}t} &= \frac{c_{\mathrm{NO}_2} c_{\mathrm{O}_2} c_{\mathrm{NOB}}}{(\omega_{NB} c_{\mathrm{NO}_2} + 1)(\omega_{GB} c_{\mathrm{O}_2} + 1)} - c_{\mathrm{NOB}}, \\
\epsilon\lambda_X c_{\mathrm{XOB}t} &= \frac{c_{\mathrm{NO}_2} c_{\mathrm{NH}_4} c_{\mathrm{XOB}}}{(c_{\mathrm{NH}_4} + \Omega_{AX})(\omega_{NX} c_{\mathrm{NO}_2} + 1)} \eta - c_{\mathrm{XOB}},
\end{aligned}
\tag{3.3}
$$

where the parameters remain unchanged from Eq. 2.15 and we introduce the new parameters

$$
\nu = \frac{D_G t_0}{L^2}, \quad \delta_J = \frac{D_J}{D_G}. \tag{3.4}
$$

Typical values for diffusion coefficients in water are $D_G = 2 \times 10^{-9}$ m^2 s^{-1}, $D_A = 1.86 \times 10^{-9}$ m^2 s^{-1}, and $D_N = D_P = 1.7 \times 10^{-9}$ m^2 s^{-1} (Kreft et al. 2001). These values do not reflect modifications due to porosity, tortuosity, and ionic charge.

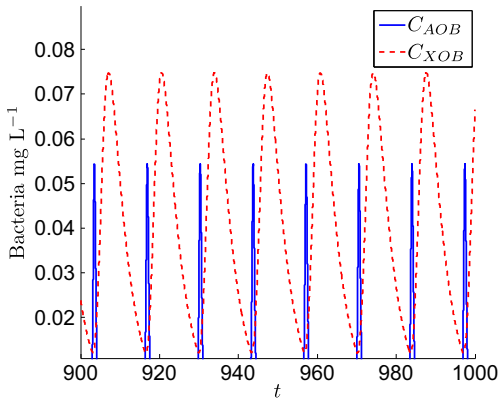

Fig. 5 C_{AOB} (*Nitrosomonas*) and C_{XOB} (*B. anammoxidans*) bacterial populations in mg L^{-1} displayed together to demonstrate the phase shift in their oscillations

We introduce the non-dimensional boundary oxygen value $\mathcal{G} = \frac{\bar{C}_{\mathrm{O}_2}}{C^0_{\mathrm{O}_2}}$. Table 3 lists the new parameter values based on the listed diffusion coefficients and the time scale in Table 2.

We simulate the model (3.3) using a method of lines procedure (Schiesser 1991) with cell-centred finite differences in the spatial variable. Using this method reduces the partial differential equations to a set of ordinary algebraic differential equations in time only. As such the

Table 3 Diffusion parameter values

Symbol	Value
ν	0.91×10^{-2}
$\delta_N = \delta_P$	0.85
δ_A	0.93
$\mathcal{G}$	2.04

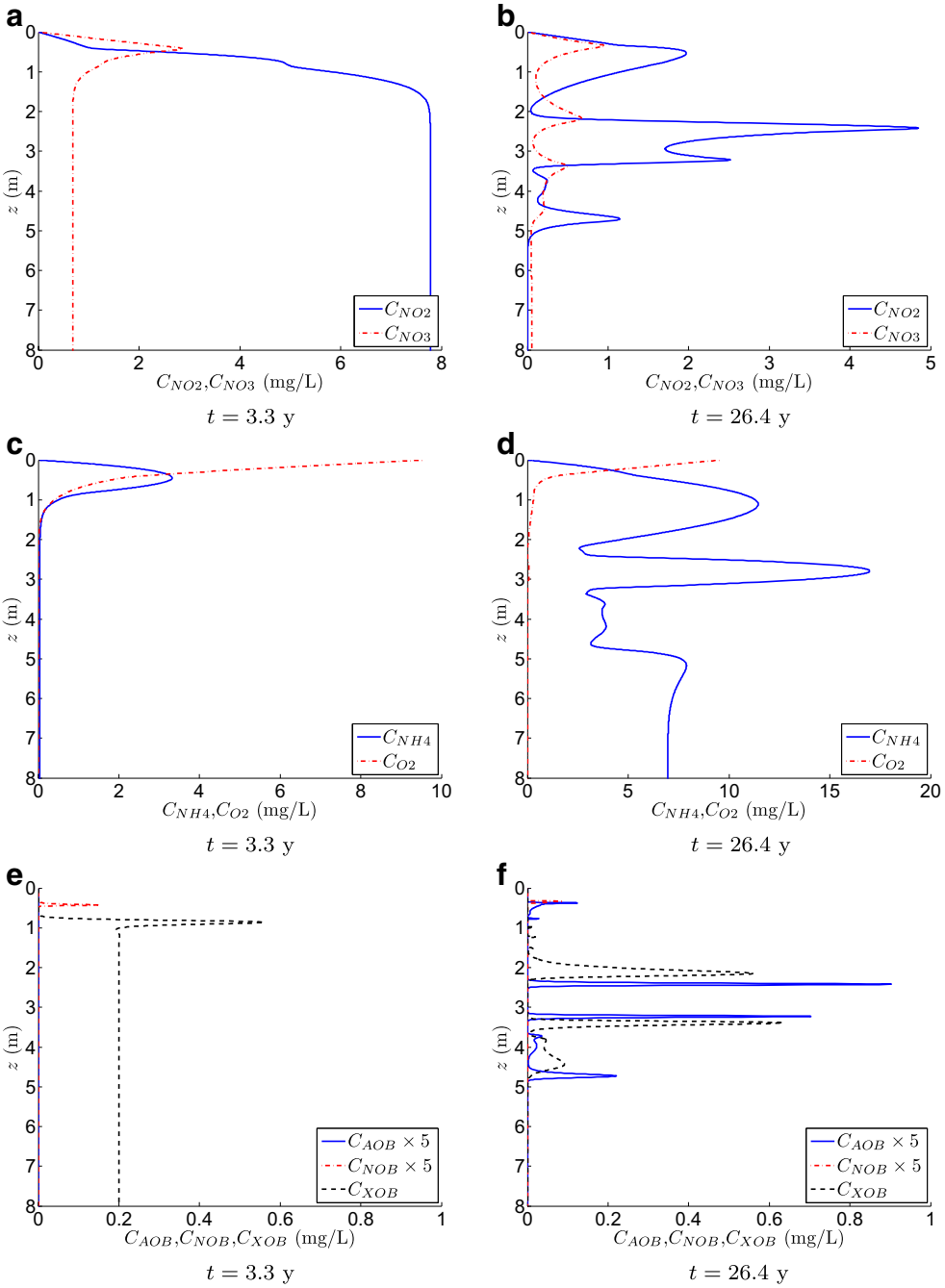

Fig. 6 Numerical simulations of Eq. 3.3 for nutrients N (nitrite), P (nitrate), A (ammonium), G (oxygen) and bacteria S (*Nitrosomonas*), B (*Nitrobacter*), and X (*B. anammoxidans*). The parameters are chosen from Tables 2 and 3. The time for each simulation is 3.3 years for panel (**a**), (**c**), and (**e**) and 26.4 years for panels (**b**), (**d**), and (**f**)

MATLAB solver `ode45` is available for the time-dependent equations that result. A similar numerical framework was used for the spatial carbon cycling model in McGuinness et al. (2014). We take a spatial mesh on $[0, 20]$ with step size 5×10^{-3} and take care that the final computational time is sufficiently small that artificial reflections do not occur from the travelling waves reaching the right boundary. We initialise the bacterial populations with the value 1×10^{-6} and use the parameter set taken from Tables 2 and 3 recalling that the values of λ_X and γ_N fall within the weak instability band (2.19) of the chemostat model (2.16). Since the ω_{ij} and Ω_{ij} are small values for ammonium and nitrite, then the full spatial system (3.3) should induce travelling waves in regions of low oxygen as would be expected for Eq. 2.16 with the addition of diffusion. The simulation results for $C_{\mathrm{NO_2}}$, $C_{\mathrm{NH_4}}$, $C_{\mathrm{O_2}}$, $C_{\mathrm{NO_3}}$, C_{AOB}, C_{NOB}, and C_{XOB} are in Fig. 6. The times plotted correspond to 3.3 years (left figures) and 26.4 years (right figures).

At $t = 3.3$ years, the constant supply of oxygen has initiated aerobic growth of the bacteria and a nitrate spike has emerged. In the anaerobic region, the ammonium has been consumed and some constant nitrite, nitrate, and

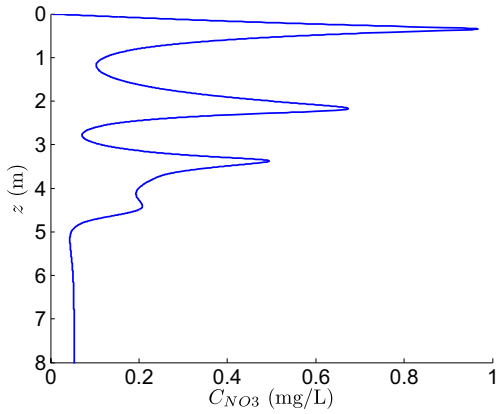

Fig. 7 Nitrate data from Fig. 6b replotted to illuminate the oscillatory behaviour

anammox bacteria have formed. Later on, at 26.4 years, the oscillations in the nutrients are fully underway and a travelling wave behaviour is observed. Regarding nitrate, the amplitude of each successive spike is smaller as they go deeper into the soil. Furthermore, the C_{AOB} and C_{XOB} bacterial peaks appear spatially out of phase with one another. Each of these features is present in Fig. 2. To emphasise the nitrate spikes at 26.4 years we plot the nitrate data on a smaller y-scale in Fig. 7. According to Fig. 6d, the oxygen has effectively been depleted by 2 m below the water table surface. However, Fig. 7 indicates that high-amplitude oscillations continue to persist as is predicted by both the data in Fig. 2b and the reduced model (2.16).

Discussion and conclusion

We investigated a bacterially mediated chemical system for nitrification involving aerobic and anaerobic reactions and showed that stable periodic solutions can be obtained in a chemostat reactor for a reduced anaerobic model. We then adapted this model to a one-dimensional soil profile where vertical diffusion was included and travelling wave behaviour was observed. Oscillatory behaviour was an anticipated result based on the data presented in Smits et al. (2009) and redrawn in Fig. 2; however, it is fairly surprising that a model as simple as Eq. 2.7 and even the reduced anoxic model (2.16) were sufficient to see such oscillations. The biochemistry of soil ecosystems is quite complex and there are several species of bacteria as well as a large cascade of redox reactions which are not modelled here. Even in the process of nitrification, there are several species capable of both aerobic and anaerobic nitrifying and denitrifying reactions including lithotrophs, such as the bacteria described in our model, but also heterotrophic bacteria which require complex carbon sources along with nitrogen (Schmidt et al. 2001b; Verhagen and Laanbroek 1991; Verhagen et al. 1992). However, even within this complex myriad of chemistry and biology, our model posits that it is sufficient to obtain oscillatory behaviour with a single representative biological process for each of nitritation and nitratation in the aerobic and anaerobic regimes. While not shown here, if values for γ_N are taken inside the weak instability band (2.19) but sufficiently far from the boundaries, then period doubling and chaotic type behaviour can be observed. This seems to be consistent with conclusions of Huisman and Weissing (1999) where chaotic oscillations were observed with plankton competition. It is worthwhile investigating and quantifying the transition from stable oscillations to apparently chaotic behaviour in this model.

Analysing the chemostat model (2.14) for zero oxygen input resulted in a simple reduced model (2.16) for the oxygen-depleted state and we were able to explicitly determine the conditions which admit stable periodic solutions (Appendix A). This anoxic state is very significant because looking at the oxygen data in Fig. 2b, it is clear that most of the soil region is anaerobic aside from a sharp, non-oscillatory diffusion layer at the phreatic surface. Furthermore, looking at other nutrients in Fig. 2 shows that oscillations occur well within the anaerobic layer. This oscillatory behaviour is also exhibited by the bacterial populations in Fig. 3. Combining this information suggests that if reaction kinetics are responsible for spatial oscillations, then it must be the anoxic kinetics which is responsible; this is quite counterintuitive since aerobic nitrification is a much larger producer of nitrate. Indeed, if we look at the data in Fig. 2a and the results of our model in Fig. 6, there is a large spike of nitrate from the aerobic activity which is primarily due to a localised cluster of nitrite-oxidising bacteria *Nitrobacter*.

It is intriguing that even though anaerobic kinetics dominate, there will always be a niche region for the oxygen-dependent nitrite oxidisers. Although it is speculated that anammox bacteria outcompete NOB for nitrite and AOB outcompete NOB for oxygen, the benefit to the NOB *Nitrobacter* seems to be in exploiting the ammonium competition between *Nitrosomonas* and *B. anammoxidans* and the oxygen inhibition of *B. anammoxidans*. Conversely in the oxygen-limited regime, the anammox bacteria are able to exploit the competition for limited oxygen supply between *Nitrosomonas* and *Nitrobacter*. Ultimately then it appears the ability for *Nitrosomonas* bacteria to thrive in both oxygen-rich and oxygen-depleted environments allows the two species *Nitrobacter* and *B. anammoxidans* to exist in separate environments.

There has been recent evidence due to Schmidt et al. (2001b) that the *Nitrosomonas* bacteria may not actually be switching biological mechanism for aerobic and anaerobic

ammonium oxidation but rather are always using NO_2 gas as a nutrient in place of oxygen. It was observed by Schmidt et al. (2001a) and Zart et al. (2000) that aerobic nitrification was inhibited when gaseous NO_2 was removed from laboratory cultures and similarly Schmidt et al. (2001c) and Zart and Bock (1998) showed that nitrogenous oxides have a promoting effect on pure cultures of a *Nitrosomonas* species. It is known (Schmidt et al. 2001b) that even in classic aerobic nitrification, hydroxylamine (NH_2OH) is the intermediary product in Eq. 2.1a that reacts to form nitrite. The full reaction is as follows

$$\begin{aligned} NH_4^+ + O_2 + H^+ + 2e^- &\rightarrow NH_2OH + H_2O \\ NH_2OH + H_2O &\rightarrow NO_2^- + 5H^+ + 4e^- \end{aligned} \tag{4.1}$$

and then oxygen is the terminal electron acceptor,

$$\tfrac{1}{2}O_2 + 2H^+ + 2e^- \rightarrow H_2O, \tag{4.2}$$

which summing together yields the Eq. 2.1a. However, it is proposed by Schmidt et al. (2001b) that NO_2 (or N_2O_4) replaces the oxygen in the reaction to form hydroxylamine with nitrous oxide NO as a by-product. Oxygen is still the terminal electron acceptor via (4.2) but is also used to convert NO back into NO_2. The reaction is proposed as

$$\begin{aligned} NH_4^+ + 2NO_2 + H^+ + 2e^- &\rightarrow NH_2OH + 2NO + H_2O \\ NH_2OH + H_2O &\rightarrow NO_2^- + 5H^+ + 4e^- \\ 2NO + O_2 &\rightarrow 2NO_2 \end{aligned} \tag{4.3}$$

which also combines with Eq. 4.2 to yield the identical net C_{AOB} mediated reaction (2.1a). When oxygen is not available for *Nitrosomonas*, the ammonium oxidation reaction in Eq. 4.3 is unaffected as is the nitrite production reaction but instead the NO remains as a by-product and nitrite acts as a partial electron acceptor in place of water with nitrogen gas emitted as a product. However, as the full anaerobic reaction Eq. 2.4 indicates, nitrite is still ultimately produced. Therefore, since the base reaction from the perspective of *Nitrosomonas* remains unchanged with or without sufficient oxygen supply, then as long as there is sufficient ammonium to consume, the bacteria need not worry about the oxygen level of their environment. It is worth reemphasising that the borehole data does not provide evidence of the presence of NO_2; however, the key insight from Eq. 4.3 is that AOB can adapt their nutrient supply without adapting their metabolic pathway, and so long as some nutrient is available for anoxic growth, populations will be sustained in both aerobic and anaerobic regions.

It was recently proposed by Cribbin et al. (2014) that reaction fronts can form between two reactants when a secondary reaction occurs with a reactant that diffuses across the front and reforms. We have exactly such a scenario with the modified nitritation Eq. 4.3 where NO_2 is consumed and then reformed with oxygen. Therefore, it could be this process that not only separates the oxygen reaction front but also allows the transport of nitrogenous gases into the anoxic layer. Furthermore, the passive role that *Nitrosomonas* bacteria play in allowing regional coexistence of *Nitrobacter* and *B. anammoxidans* could be the bacterial front analogue to the conclusion of Cribbin et al. (2014) which would be that competing bacterial species can coexist and thrive as long as there is a third species that can thrive in each environment through passive competition. Huisman and Weissing (1999) showed that introducing competitors can lead to oscillations in populations provided that they were rate limited enough as to not exclude their competitors from a given nutrient. However, their analysis was limited to a single environment and we are considering two environments, aerobic and anaerobic saturated groundwater with nutrient exchange. We are suggesting that stable oscillations in each environment require passive competition through a species that can exist in each environment. Such a hypothesis would be worth further investigation. This important role of *Nitrosomonas* bacteria in the population dynamics of *Nitrobacter* and *B. anammoxidans* is clear from Fig. 6e, f where each peak in C_{AOB} has a corresponding peak in either C_{NOB} or C_{XOB} depending on the oxygen concentration. The bacterial data in Smits et al. (2009), redrawn in Fig. 3, corroborates this result where slightly out-of-phase peaks in population are observed.

An interesting feature of the model presented is the importance of treating ammonium as a finite resource. As a first approximation when modelling an ammonium spill, it is feasible to suggest ammonium levels to be constant. This has drastic effects for the spatial model (3.3) in "Spatial oscillations". Making this assumption and looking at Eq. 3.3_5 for c_{AOB} at the point $z = 0$ where the soil-air interface occurs and hence where oxygen is non-dimensionally prescribed as $c_{\mathrm{O}_2} = \mathcal{G}$ yields

$$\begin{aligned} \epsilon c_{\mathrm{AOB}t} &= c_{\mathrm{AOB}} \left(\frac{c_{\mathrm{NH}_4}\mathcal{G}}{(\omega_{AS} c_{\mathrm{NH}_4} + 1)(\mathcal{G} + \Omega_{GS})} - 1 \right) \\ &= \kappa c_{\mathrm{AOB}}, \quad z = 0. \end{aligned} \tag{4.4}$$

We have simplified $\eta \approx 0$ since the environment is quite oxygen rich here and since c_{NH_4} is assumed to be constant then κ is a constant. Either κ is positive in which case there will be infinite growth, κ is negative and the population will go extinct or $\kappa \equiv 0$ and the population is static. Instead, by including c_{NH_4} in the model, it allows for a zero boundary condition at $z = 0$ which prohibits bacterial growth there and nutrients, such as the oxic nitrate spike, would form

away from the origin. Indeed, this is observed in both Fig. 6 and the data in Figs. 1 and 2.

There are several avenues of future work both experimentally and mathematically that are open. Clearly, the role of NO_2 needs to be better understood in the context of soil nitrogen dynamics. Schmidt et al. (2001b) state that the ecological evidence for these nitrogenous gases is still an object of speculation and that NO_2 is not naturally available in most anoxic environments. Therefore, it must be transported from aerobic regions and the modified aerobic ammonium oxidation Eq. 4.3 could be the mechanism that allows this transfer to occur. The lack of clarity on sources and availability of NO_2 was the primary motivation for the assumption of constant levels and further experimental data would help properly incorporate this into the model. We recommend that all future borehole chemistry analyses specifically look for NO_2 (and ideally other important nitrogenous gases such as NO). This would help elucidate the conclusion from our model that the majority of the dynamics happen in the anoxic layer as a consequence of such gases. It has been shown by Schmidt and Bock (1997) that NO, which is a product of the anaerobic nitrite production (2.4), may inhibit NO_2 activity of *Nitrosomonas*. However, it has also been shown by Kartal et al. (2010) that NO does not inhibit anammox bacteria and that they can use this gas to oxidise additional ammonium, thus removing it from the system. This could be a potential method for controlling NO_2 levels and also for increasing the activator-inhibitor behaviour of the two bacteria. This could further enhance the spatial phase separation of *Nitrosomonas* and anammox bacteria. Better information about the role of NO_2 in soil bacteria metabolism would help relax the assumption that it is not rate limited and allow it to be incorporated into the model in a more complete way with the other nutrients.

Mathematically, it would be of interest to incorporate the role of hydrogen ions and pH into a nitrate model. Figure 1 shows experimentally that the concentration of hydrogen ions decreases in a similar fashion to nitrate and both deplete at the same time. Hydrogen could be a key mediator that separates anaerobic regions where nitrate is highly produced and where it is not. As well, the anaerobic nitrate reactions may play a role in maintaining necessary soil pH levels by controlling hydrogen concentrations. The mathematics of including hydrogen would be complicated as enzymatic activity can be strongly pH dependent and shifting the pH slightly can alter bacterial community structures. An empirical equation for pH has been included in Maggi et al. (2008) as a piecewise linear function but there is limited discussion on the impact on the nitrification process.

We considered nutrient transport in saturated groundwater on the basis that borehole data in Figs. 1 and 2 were provided for depths below the water table. This is not meant to imply that unsaturated contaminant flow is of secondary concern; indeed, the opposite is true as groundwater pollution should be remediated in unsaturated regions before it can alter the saturated water chemistry leading to large-scale health impacts and high environmental impact and financial costs. Maggi et al. (2008) provide a mechanistic model for contaminant transport that couples to a model for water flow in the unsaturated region. Similar models are derived in Morrissey et al. (2015) for contamination due to septic tanks, although the modelling of contaminant transport is not considered in as much detail as the groundwater flow itself. In both cases, a modelling approach similar to what is presented here could not only identify the dominant contaminant transport processes and chemistry and quantify transitions such as oscillations but also target strategies for remediation in terms of soil properties and pollutant sources. This is an interesting and important future research direction.

We reemphasise that our goal for this model was not to reproduce the data set presented in Smits et al. (2009), nor any other data set, but rather to address some of the more qualitative structures found in borehole data. Our model is a fairly simple one in regard to the complex biochemistry in soil, and the core mechanics of oscillation can be explained by an even simpler model (2.16) which can be studied analytically. This simple model, when combined with scalar, one-dimensional diffusion, is able to reproduce travelling wave structures such as those seen in Fig. 2 and bacterial population peaks such as those in Fig. 3. Our model accurately captures the relevant wavelengths with peak separation between 1 to 2 m in both data and simulation. Furthermore, the oscillations appearing around 26 years is consistent with observations of dynamic behaviour in the first borehole measurements occurring approximately 20 years after the plant had closed.

The scales for the model were chosen to ensure that the terms in the proposed kinetic reactions were of comparable order, and the resulting scales were thus unrelated to the observed orders of magnitude of the chemical concentrations. Despite this, both the simulations for oxygen and nitrite produce results with comparable scales to the data in Fig. 2. Of particular interest is the agreement with the nitrite data; the scale is chosen based on the anaerobic kinetics and is an order of magnitude smaller than that suggested by the data. However, both the simulations and data suggest that the large supply of nitrite is driven into the anaerobic layer by diffusion and that a much smaller scale drives the oscillatory behaviour.

The ammonium scale and thus the nitrate scale are not commensurate with the borehole data; however, we recover the qualitative features of the observed nitrate profile, in which successive spikes decrease in amplitude with depth,

and that the anaerobic spikes have a significantly smaller concentration than the aerobic ones. The disagreement in ammonium scales is not surprising as the data belongs to an ammonium contaminant site which would be an unnatural environment compared to that of an uncontaminated site. Various values of the ammonium saturation constant ranging from 0.25 mg L^{-1} (Koops and Pommerening-Röser 2001) to 36.08 mg L^{-1} (Laanbroek et al. 1994) have been reported, and this is something that can be drastically affected by the ammonium supply conditions. The first borehole data was not recorded until 20 years after the Rexco plant had shut down, and 60 years after it first opened, and an ammonium leak over this time scale could significantly alter the ecological environment and affect all of the model parameters. Furthermore, by simplifying the nitrogen fixation, we would anticipate errors in the nitrate and hence ammonium scales, as nitrate is the key terminal electron acceptor for denitrification. This only further validates the importance of choosing scales based on the chosen model rather than solely on the data, as the data will include processes which have not been modelled, and which can misrepresent the resulting analysis. It would be of interest to determine the kinetic parameters of Table 1 for the Rexco contaminant zone and use these for further numerical simulations.

Funding information A. C. F. receives support from the Mathematics Applications Consortium for Science and Industry (www.macsi.ul.ie) funded by the Science Foundation Ireland grant 12/IA/1683. The research is supported by Science Foundation Ireland under grant numbers SFI/09/IN.1/I2645 and SFI/13/IA/1923.

Appendix A: Linear stability analysis

To generate the instability band (2.19), we linearise (2.18) around the steady state $\theta = \phi = 0$ with eigenfunctions proportional to $e^{\sigma t}$ and eigenvalue σ which leads to the solvability condition for σ,

$$\lambda_X\sigma^4 + \epsilon\left(\tfrac{33}{124}\gamma_N\lambda_X + \tfrac{99}{124}\lambda_X\right)\sigma^3 + \left(\tfrac{99}{124}\lambda_X + \tfrac{33}{124}\gamma_N + \epsilon^2\tfrac{33}{124}\gamma_N\lambda_X\right)\sigma^2 + \epsilon\tfrac{33}{124}\gamma_N(\lambda_X+1)\sigma + \tfrac{33}{124}\gamma_N = 0. \quad \text{(A.1)}$$

We exploit the starvation limit $\epsilon \ll 1$ and consider a two-term regular expansion for $\sigma \sim \sigma_0 + \epsilon\sigma_1$ for reasons that will become clear. The leading order eigenvalue problem for $\mu = \sigma_0^2$ satisfies

$$\lambda_X\mu^2 + \left(\tfrac{33}{124}\gamma_N + \tfrac{99}{124}\lambda_X\right)\mu + \tfrac{33}{124}\gamma_N = 0, \quad \text{(A.2)}$$

the solution of which leads to either real, negative roots or complex roots with negative real part for μ. The complex eigenvalues exist provided $\lambda_X > 1$ and

$$\underbrace{\left(\tfrac{149}{33} - \tfrac{20}{33}\sqrt{31}\right)\lambda_X}_{\gamma_N^-} < \gamma_N < \underbrace{\left(\tfrac{149}{33} + \tfrac{20}{33}\sqrt{31}\right)\lambda_X}_{\gamma_N^+}. \quad \text{(A.3)}$$

For γ_N in this range, σ_0 is complex with a positive real value and hence (A.3) forms an instability band. Outside this band, the eigenvalue Eq. A.2 produces σ_0 as purely imaginary conjugate pairs. An example of this bifurcation at γ_N^- and γ_N^+ for $\lambda_X = 41.67$ is in Fig. 8. Here, μ^+ is the eigenvalue associated with the positive square root solution to Eq. A.2 and μ^- the negative square root.

The value of γ_N in Table 2 is below the bifurcation threshold γ_N^- and at first the problem, as posed, would

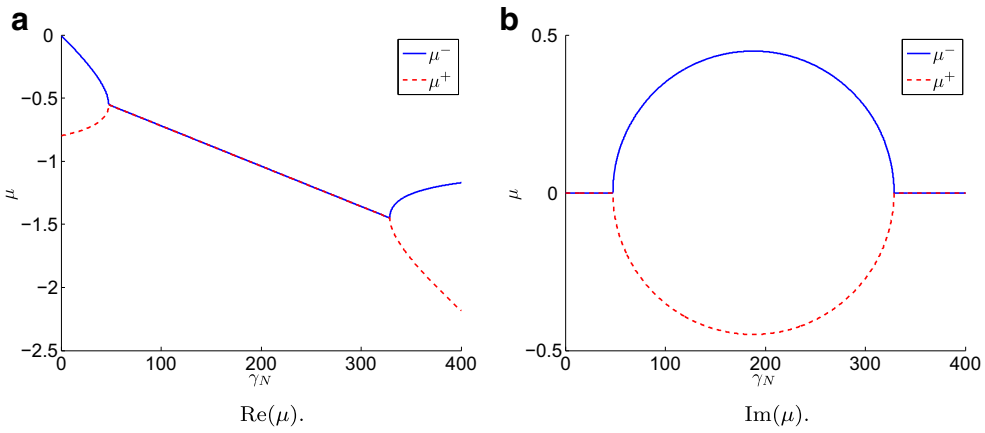

Fig. 8 Eigenvalues $\mu = \sigma_0^2$ corresponding to the solution of Eq. A.2 with $\lambda_X = 41.67$. The real component of the eigenvalues are in (**a**) while the imaginary are in (**b**)

appear stable. However, the correction σ_1 will introduce the instability into the problem. The σ_1 correction satisfies

$$\sigma_1 = -\frac{33}{2}\frac{\lambda_X\gamma_N + 3\lambda_X\mu + \mu\gamma_N\lambda_X + \gamma_N}{248\lambda_X\mu + 33\gamma_N + 99\lambda_X}, \tag{A.4}$$

with μ the solution of Eq. A.2. When σ_0 is purely imaginary, then μ is real and σ_1 is real and therefore provides the leading order real behaviour. The stability boundary then comes from setting σ_1 to zero which yields

$$\gamma_N\left[\tfrac{33}{25}\gamma_N^2 - \left(\lambda_X^2 + \tfrac{248}{25}\lambda_X + 1\right)\gamma_N + \tfrac{297}{25}\lambda_X^2\right] = 0, \tag{A.5}$$

and this produces the non-trivial roots,

$$\bar{\gamma}_N^{\pm} = \tfrac{25}{66}\left(\lambda_X^2 + \tfrac{248}{25}\lambda_X + 1 \pm \tfrac{(\lambda_X+1)}{5}\sqrt{25\lambda_X^2 + 446\lambda_X + 25}\right) \tag{A.6}$$

which appear in Eq. 2.19. Since these roots exist when σ_0 is purely imaginary then necessarily, $\bar{\gamma}_N^- < \gamma_N^-$ and $\bar{\gamma}_N^+ > \gamma_N^+$. Combining this with Eq. A.3, we recover (2.19), i.e. that the base state $(\theta, \phi) = (0, 0)$ is unstable if

$$\bar{\gamma}_N^- < \gamma_N < \bar{\gamma}_N^+. \tag{A.7}$$

We refer to the instability region (A.3) as the strong instability band because, if satisfied, the $(0, 0)$ base state will be unstable even for $\epsilon = 0$ exactly. However, when ϵ is finite but small, then the instability band extends to Eq. 2.19 which we denote the weak instability band. Using the values in Table 2 yields $\bar{\gamma_N}^- = 9.65$ and $\bar{\gamma}_N^+ = 1.62 \times 10^3$. Solving the roots of Eq. A.1 numerically using $\epsilon = 0.1$ as in Table 2 yields the true instability threshold,

$$11.03 < \gamma_N < 91.95, \tag{A.8}$$

which is in fair agreement with the lower bound $\bar{\gamma}_N^-$ from the asymptotic analysis. The source of error in the upper bound is due to $\bar{\gamma}_N^+$ being of $\mathcal{O}(\epsilon^{-1})$ and a proper rescaling of γ_N would be required to accurately asymptotically approximate the upper band for such a large value of ϵ. However, this is mitigated for smaller values of ϵ as seen in Table 4 where the value of λ_X is once again taken from Table 2.

Table 4 Numerical instability bounds to γ_N

ϵ	Lower	Upper
0.1	11.03	91.95
0.01	9.66	1.37×10^3
0.001	9.65	1.62×10^3
0.0001	9.65	1.62×10^3

References

Alfreider A, Krössbacher M, Psenner R (1997) Groundwater samples do not reflect bacterial densities and activity in subsurface systems. Water Res 31(4):832–840

Bailey RT, Gates TK, Romero EC (2015) Assessing the effectiveness of land and water management practices on nonpoint source nitrate levels in an alluvial stream–aquifer system. J Contam Hydrol 179:102–115

Barber SA (1995) Soil nutrient bioavailability: a mechanistic approach. Wiley, New York

Blackburne R, Vadivelu VM, Yuan Z, Keller J (2007) Determination of growth rate and yield of nitrifying bacteria by measuring carbon dioxide uptake rate. Water Environ Res: A Res Publ Water Environ Federation 79(12):2437–2445

Broholm MM, Jones I, Torstensson D, Arvin E (1998) Groundwater contamination from a coal carbonization plant. Geol Soc, Lond, Eng Geology Special Publ 14(1):159–165

Capuno REJr (2007) Mathematical modeling for nitrogen removal via a nitritation: anaerobic ammonium oxidation-coupled biofilm in a hollow fiber membrane bioreactor and a rotating biological contactor. Master's thesis, Virginia Polytechnic Institute and State University

Charoanwoodtipong T, Limpiyakorn T, Suwannasilp BB (2015) Kinetics of ammonia-oxidizing microorganisms and nitrite-oxidizing bacteria enriched at high and low ammonia concentrations. In: Proceedings of the 3rd International Conference on Biological, Chemical and Environmental Sciences, pp 1–5

Cribbin LB, Winstanley HF, Mitchell SL, Fowler A, Sander GC (2014) Reaction front formation in contaminant plumes. J Contam Hydrol 171:12–21

Davison R (1998) Natural attenuation and risk assessment of groundwater contaminated with ammonium and phenolics. PhD thesis, University of Bradford

Fowler A (2011) Mathematical geoscience, vol 36. Springer Science & Business Media, Berlin

Fowler A (2014) Starvation kinetics of oscillating microbial populations. Math Proc R Ir Acad 114(2):173–189

Fowler A, Winstanley HF, McGuinness MJ, Cribbin LB (2014) Oscillations in soil bacterial redox reactions. J Theor Biol 342:33–38

Gleeson T, Befus KM, Jasechko S, Luijendijk E, Cardenas MB (2015) The global volume and distribution of modern groundwater. Nature Geoscience, Advance on(November):1–15

Hanaki K, Wantawin C, Ohgaki S (1990) Nitrification at low levels of dissolved oxygen with and without organic loading in a suspended-growth reactor. Water Res 24(3):297–302

Helder W, De Vries R (1983) Estuarine nitrite maxima and nitrifying bacteria (ems-dollard estuary). Neth J Sea Res 17(1):1–18

Huisman J, Weissing FJ (1999) Biodiversity of plankton by species oscillations and chaos. Nature 402(6760):407–410

Johnsson H, Bergstrom L, Jansson P-E, Paustian K (1987) Simulated nitrogen dynamics and losses in a layered agricultural soil. Agric Ecosyst Environ 18(4):333–356

Kartal B, Tan NCG, Van Biezen ED, Kampschreur MJ, Van Loosdrecht MCM, Jetten MSM (2010) Effect of nitric oxide on anammox bacteria. Appl Environ Microbiol 76(18):6304–6306

Kindred JS, Celia MA (1989) Contaminant transport and biodegradation: 2. Conceptual model and test simulations. Water Resour Res 25(6):1149–1159

Kinzelbach W, Schäfer W, Herzer J (1991) Numerical modeling of natural and enhanced denitrification processes in aquifers. Water Resour Res 27(6):1123–1135

Kogure K, Koike I (1987) Particle counter detrmination of bacterial biomass in seawater. Appl Environ Microbiol 53(2):274–277

Koops HP, Pommerening-Rˆoser A (2001) Distribution and ecophysiology of the nitrifying bacteria emphasizing cultured species. FEMS Microbiol Ecol 37(1):1–9

Kopell N, Howard L (1973) Plane wave solutions to reaction-diffusion equations. Stud Appl Math 52(4):291–328

Kreft JU, Picioreanu C, Wimpenny JW, van Loosdrecht MC (2001) Individual-based modelling of biofilms. Microbiology (Reading, England) 147(Pt 11):2897–912

Laanbroek HJ, Bodelier PLE, Gerards S (1994) Oxygen consumption kinetics of Nitrosomonas europaea and Nitrobacter hamburgensis grown in mixed continuous cultures at different oxygen concentrations. Arch Microbiol 161(2):156–162

Langergraber G, Rousseau DPL, Garcia J, Mena J (2009) CWM1: A general model to describe biokinetic processes in subsurface flow constructed wetlands. Water Sci Technol 59(9):1687–1697

Maggi F, Gu C, Riley W, Hornberger G, Venterea R, Xu T, Spycher N, Steefel C, Miller N, Oldenburg C (2008) A mechanistic treatment of the dominant soil nitrogen cycling processes: model development, testing, and application. J Geophys Res Biogeosci 113(G2)

McGuinness MJ, Cribbin LB, Winstanley HF, Fowler A (2014) Modelling spatial oscillations in soil borehole bacteria. J Theor Biol 363:74–79

Mekala C, Gaonkar O, Nambi IM (2017) Understanding nitrogen and carbon biogeotransformations and transport dynamics in saturated soil columns. Geoderma 285:185–194

Michaelis L, Menten ML (1913) Die kinetik der invertinwirkung. Biochem z 49(333-369):352

Monod J (1949) The growth of bacterial cultures. Annu Rev Microbiol 3(1):371–394

Morrissey P, Johnston P, Gill L (2015) The impact of on-site wastewater from high density cluster developments on groundwater quality. J Contam Hydrol 182:36–50

Mulder A, van de Graaf AA, Robertson L, Kuenen J (1995) Anaerobic ammonium oxidation discovered in a denitrifying fluidized bed reactor. FEMS Microbiol Ecol 16(3):177–183

Munz G, Lubello C, Oleszkiewicz JA (2011) Factors affecting the growth rates of ammonium and nitrite oxidizing bacteria. Chemosphere 83(5):720–725

Nowka B, Daims H, Spieck E (2015) Comparison of oxidation kinetics of nitrite-oxidizing bacteria: nitrite availability as a key factor in niche differentiation. Appl Environ Microbiol 81(2):745–753

Oshiki M, Shimokawa M, Fujii N, Satoh H, Okabe S (2011) Physiological characteristics of the anaerobic ammonium-oxidizing bacterium 'Candidatus Brocadia sinica'. Microbiology 157(6):1706–1713

Ranjbar F, Jalali M (2013) Measuring and modeling ammonium adsorption by calcareous soils. Environ Monit Assess 185(4):3191–3199

Salem S, Moussa MS, van Loosdrecht MCM (2006) Determination of the decay rate of nitrifying bacteria. Biotechnol Bioeng 94(2):252–62

Sander R (2015) Compilation of henry's law constants (version 4.0) for water as solvent. Atmos Chem Phys 15(8)

Scaglione D, Caffaz S, Bettazzi E, Lubello C (2009) Experimental determination of Anammox decay coefficient. J Chem Technol Biotechnol 84(8):1250–1254

Schiesser WE (1991) The numerical method of lines. Academic Press, Cambridge

Schmidt I, Bock E (1997) Anaerobic ammonia oxidation with nitrogen dioxide by Nitrosomonas eutropha. Arch Microbiol 167(2-3):106–111

Schmidt I, Bock E (1998) Anaerobic ammonia oxidation by cell-free extracts of Nitrosomonas eutropha. Anton Leeuw Int J Gen Mol Microbiol 73(3):271–278

Schmidt I, Bock E, Jetten MS (2001a) Ammonia oxidation by nitrosomonas eutropha with no2 as oxidant is not inhibited by acetylene. Microbiology 147(8):2247–2253

Schmidt I, Sliekers AO, Schmid MC, Cirpus I, Strous M, Bock E, Kuenen JG, Jetten MSM (2001b) Aerobic and anaerobic ammonia oxidizing bacteria competitors or natural partners? FEMS Microbiol Ecol 39(3):175–181

Schmidt I, Zart D, Bock E (2001c) Effects of gaseous NO2 on cells of nitrosomonas eutropha previously incapable of using ammonia as an energy source. Antonie Van Leeuwenhoek 79(1):39–47

Sliekers AO, Haaijer SCM, Stafsnes MH, Kuenen JG, Jetten MSM (2005) Competition and coexistence of aerobic ammonium- and nitrite-oxidizing bacteria at low oxygen concentrations. Appl Microbiol Biotechnol 68(6):808–817

Smits THM, Hùttmann A, Lerner DN, Holliger C (2009) Detection and quantification of bacteria involved in aerobic and anaerobic ammonium oxidation in an ammonium-contaminated aquifer. Bioremediation J 13(1):41–51

Strohm TO, Griffin B, Zumft WG, Schink B (2007) Growth yields in bacterial denitrification and nitrate ammonification. Appl Environ Microbiol 73(5):1420–1424

Strous M, Heijnen J, Kuenen JG, Jetten MSM (1998) The sequencing batch reactor as a powerful tool for the study of slowly growing anaerobic ammonium-oxidizing microorganisms. Appl Micorbial biotechnol 50:589–596

Van der Heijden R, Heijnen J, Hellinga C, Romein B, Luyben K (1994) Linear constraint relations in biochemical reaction systems: i. Classification of the calculability and the balanceability of conversion rates. Biotech Bioeng 43(1):3–10

Verhagen FJ, Laanbroek HJ (1991) Competition for ammonium between nitrifying and heterotrophic bacteria in dual energy-limited chemostats. Appl Environ Microbiol 57(11):3255–3263

Verhagen FJM, Duyts H, Laanbroek HJ (1992) Competition for ammonium between nitrifying and heterotrophic bacteria in continuously perculated soil columns. Appl Environ Microbiol 58(11):3303–3311

Whitman WB, Coleman DC, Wiebe WJ (1998) Prokaryotes: the unseen majority. Proc Natl Acad Sci 95(12):6578–6583

Widdowson MA, Molz FJ, Benefield LD (1988) A numerical transport model for oxygen-and nitrate-based respiration linked to substrate and nutrient availability in porous media. Water Resour Res 24(9):1553–1565

Wiesmann U (1994) Biological nitrogen removal from wastewater. In: Biotechnics/wastewater. Springer, pp 113–154

Wrage N, Velthof GL, Van Beusichem ML, Oenema O (2001) Role of nitrifier denitrification in the production of nitrous oxide. Soil Biol Biochem 33(12-13):1723–1732

Yu XF, Zhang YX, Zou YC, Zhao HM, Lu XG, Wang GP (2011) Adsorption and desorption of ammonium in wetland soils subject to freeze-thaw cycles. Pedosphere 21(2):251–258

Zart D, Bock E (1998) High rate of aerobic nitrification and denitrification by Nitrosomonas eutropha grown in a fermentor with complete biomass retention in the presence of gaseous NO2 or NO. Arch Microbiol 169(4):282–286

Zart D, Schmidt I, Bock E (2000) Significance of gaseous no for ammonia oxidation by nitrosomonas eutropha. Antonie Van Leeuwenhoek 77(1):49–55